

Energy Neutral Sensor System With Micro-scale Photovoltaic and Thermoelectric Energy Harvesting

Anand Savanth^{1,3}, Mathieu Bellanger², Alex Weddell¹, James Myers³
and Mathias Kauer²

¹ University of Southampton, Southampton, UK

² Lightricity Ltd, Oxford, UK

³ ARM Ltd, Cambridge, UK

E-mail: anand.savanth@arm.com

Abstract. Minimizing power conversion losses is critical for energy neutral operation of micro-scale energy harvested sensor nodes. These small form-factor sensor nodes rely on miniature harvesters with low output voltages that must be boosted with large conversion ratios to recharge batteries or super-capacitors. Selective Direct Operation (SDO), a technique to selectively avoid power conversion and thereby eliminate conversion loss in energy harvested systems has been demonstrated as an effective technique for light harvesters. This paper extends SDO to thermoelectric generators (TEGs). SDO exploits the ultra-low circuit functional voltages, enabling sensor systems to effectively harvest energy from cm-scale TEGs which output few 10's of mW but at low output voltages (100's of mV). PV cell construction from prior-work, TEG characterization and field measurements are presented in this paper to demonstrate the effectiveness of SDO and co-designing energy harvesters, power conversion circuits and digital sub-systems.

1. Introduction

Modern circuit design and silicon fabrication techniques have made possible ultra-low power miniature sensor systems with sufficient compute capability to enable the Internet of Things - specifically the leaf nodes that generate vast sensor data. A common theme of these techniques is aggressive and fast supply voltage scaling as lower voltage results in quadratic reduction in expended power. However, as demonstrated consistently by prior works [1][2][3][4], there exists a lower bound to the supply voltage below which operating energy increases despite an apparent reduction in power. This minimum-energy (MinE) point is determined by the static power. This is further exacerbated by heavily duty-cycled workloads in typical sensor applications.

Energy harvesting in such systems is critical to further enable untethered and extended operating periods as typical battery self-discharge is greater than the sleep power of such systems. However, this objective necessitates integrated power conversion which in practice is lossy. Typically, two stage conversion is used to 1) charge the 1.2~3.6V battery from the low voltages available from small form-factor energy harvesters and 2) to convert down from battery voltages to the low supply voltage at which MinE operation is possible. This two-stage conversion is lossy and state-of-the-art aims at high-efficiency conversion techniques at low input voltage

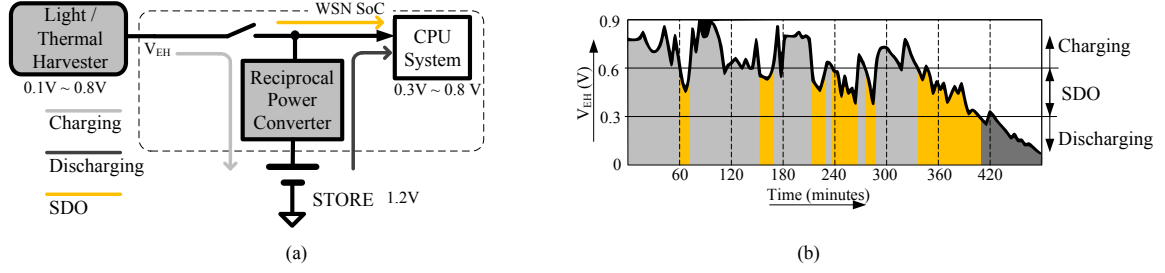


Figure 1: Selective Direct Operation [8] (a) block diagram and (b) conceptual operation

and power levels [5]. Note that conversion losses increase with conversion ratio and prior works aim to eliminate conversion stages under low input power conditions [6][7]. A related technique, Selective Direct Operation (SDO), has been demonstrated [8] with Photovoltaic (PV) cells to exploit the low operating voltage of MinE systems and minimize power conversion losses.

In this work, fabrication details of the high-efficiency PV cell are provided and the proposed SDO technique is extended to thermoelectric generators (TEGs) as an alternate source of energy harvesting. Measurements from real-world scenarios are presented supporting deployability of SDO for MinE sensor systems.

2. Power Conversion Losses and Selective Direct Operation

SDO is illustrated in Fig. 1 wherein a single reciprocal convertor is used for power conversion from harvester to battery and from battery to the CPU system. This minimizes losses associated with traditional two stage conversion. Further, at poor ambient energy levels, the system's ability to harvest energy is limited by power conversion overheads. For such conditions, SDO exploits the ultra-low operating voltage of subthreshold CPU systems to extend battery capacity by 1) direct operation of logic from harvester thereby eliminating conversion overheads and 2) avoiding battery discharge during these periods. SDO has been successfully demonstrated [8] with the MinE system executing an industry standard sensor benchmark software with ability to cold start at indoor conditions and charge a 1.2V NiMH battery when sufficient ambient energy is available.

2.1. Low-light high efficiency PV cell

The high efficiency PV cell for this work is fabricated by Lightricity. It is optimized for fluorescent and LED indoor lighting using high purity inorganic materials (Fig. 2). Measured results show $>22 \mu\text{W}/\text{cm}^2$ with 35% efficiency at 200 lux and can retain high efficiency down to very low light levels (10 lux). The low-light operating voltage (V_{MPP}) of $\sim 1\text{V}$ at 200 lux significantly eases design constraints on maximum power point tracking (MPPT) and power conversion

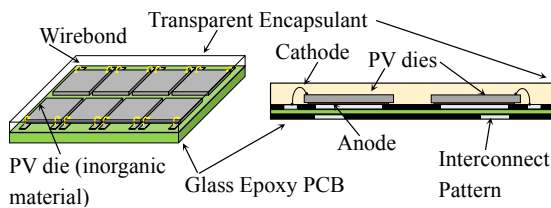


Figure 2: High efficiency PV cell for low-light conditions

Total size (mm)	: 23.8x10.2x1.5
Active area (cm^2)	: 2.15
$V_{\text{OC}}, I_{\text{SC}}$: 1.15V, 49.8 μA
$V_{\text{MPP}}, I_{\text{MPP}}$: 1V, 47.6 μA
P_{MPP}	: 47.6 μW
Power Density	: 22.1 $\mu\text{W}/\text{cm}^2$

Table 1: PV cell performance summary

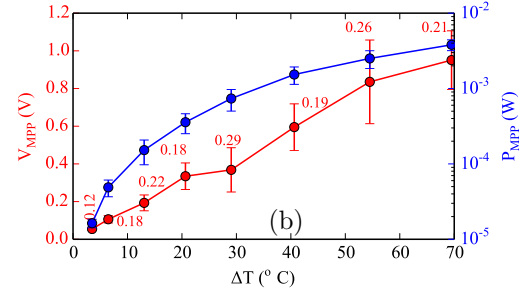
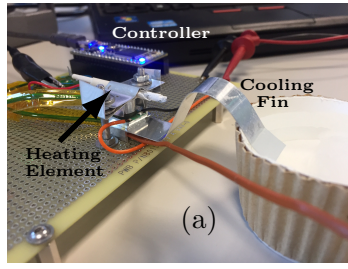


Figure 3: (a): Characterisation setup for TEG and (b): Measured power vs ΔT and variability in V_{MPP}

circuits. The PV cells have been pre-characterized to estimate the impedance vs illumination characteristics and variation-aware models have been developed to aid with power convertor circuit simulation highlighting the effectiveness of harvester and circuit co-design.

2.2. TEG characterization and measurements

Similarly, commercially available cm^3 TEGs have been characterized by emulating differential temperature surfaces using a heater and cooling-fin setup as shown in Fig 3a. The ratio of V_{MPP}/V_{OC} is ≈ 0.5 , however the ratio shows part-to-part variation and dependence on temperature (Fig 3b). The error-bars on the voltage and power trace highlight the variability observed when measuring 5 different samples for similar temperature gradients. However, the coefficient of variance (σ/μ) is 10x lower compared to commercial off-the-shelf micro-scale PV cells. Harvested power from ambient heat sources (hot-water dispenser and room radiator) is measured to be between 10-1000 μW (Fig 4).

3. Measured Results and Energy Neutral Operation

Fig. 4 shows the system block diagram along with start-up comparator and V_{MPP} tracking scheme which modulates the convertor and CPU internal clock for MPPT during charging and direct operation (Fig 1b). The convertor is implemented in $175 \times 210 \text{sq.}\mu\text{m}$ area on a $1.94 \times 1.94 \text{mm}$ chip. When harvesting from PV cells V_{EH} in Fig 5a can vary between 0 to 1.1V while it is much lower with the TEG. ΔT as high as 40°C generates $V_{MPP} < 0.6\text{V}$. SDO is more effective for these applications where the low harvester output voltages impose large conversion overheads. Fig 5c shows the oscilloscope waveforms when the CPU is in sleep and active mode showing GPIO

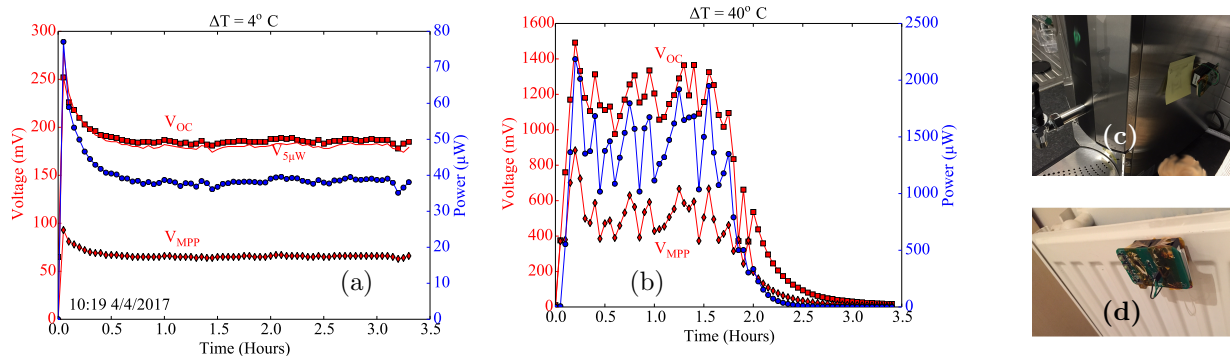


Figure 4: TEG measurements under field conditions (a,c): Low ΔT (4°C) conditions and (b,d): Large ΔT (40°C) conditions

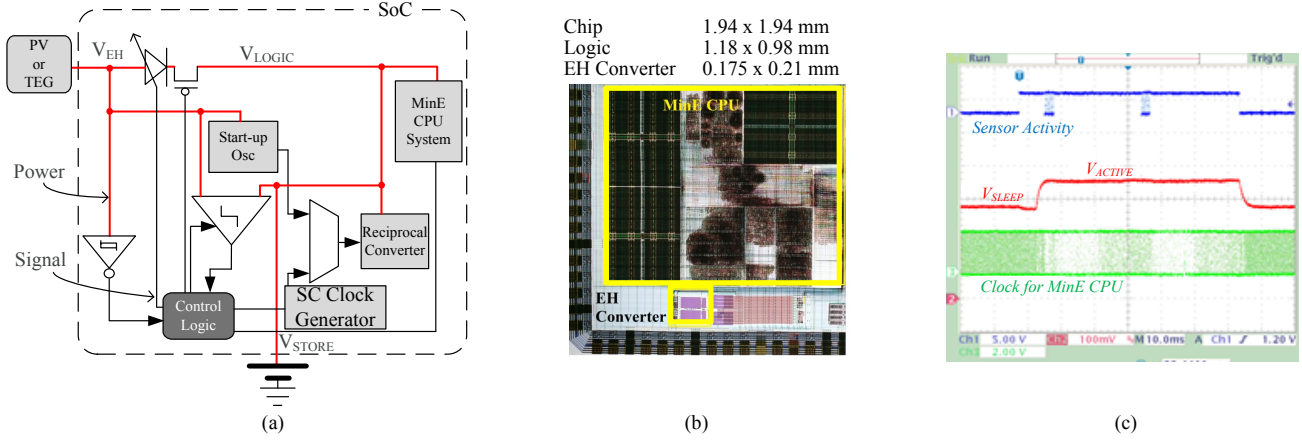


Figure 5: SoC block diagram and chip floorplan

activity in active mode. Also shown is the corresponding V_{LOGIC} and CPU clock frequency.

4. Conclusions

This paper presented experimental results demonstrating the effectiveness of co-designing energy harvesters, power conversion circuits and digital sub-systems in micro-scale energy harvesting sensor nodes. Prior work on SDO was extended by reporting harvester characterization methodology and field evaluation of SDO while harvesting from cm^3 form-factor PV cells and TEGs.

5. Acknowledgments

The authors extend thanks to Jedrzej Kufel for support with TEG measurements and characterization.

References

- [1] J. Kwong et al., "A 65nm Sub-Vt Microcontroller with Integrated SRAM and Switched-Capacitor DC-DC Converter" in IEEE Int. Solid-State 580 Circuits Conf. (ISSCC) Dig. Tech. Papers, San Francisco, CA, USA, 581 Feb. 2008, pp. 318 - 616.
- [2] M. Fojtik et al., "A Millimeter-Scale Energy-Autonomous Sensor System with Stacked Battery and Solar Cells" IEEE J. Solid-State Circuits, vol. 48, no. 3, pp. 801 - 813, Mar. 2013.
- [3] D. Bol et al., "Sleepwalker: A 25-Mhz 0.4-V Sub- mm^2 $7\mu\text{W}/\text{Mhz}$ Microcontroller in 65-Nm LP/GP CMOS For Low-Carbon Wireless Sensor Nodes" in IEEE Int. Solid-State Circuits Conf. (ISSCC) Dig. Tech. Papers, San Francisco, CA, USA, Jan. 2013, pp. 20 - 32.
- [4] J. Myers, A. Savanth, D. Howard, R. Gaddh, P. Prabhat, and D. Flynn, "An 80nw Retention 11.7pJ/cycle Active Subthreshold ARM Cortex-M0+ Subsystem in 65nm CMOS For WSN Applications" IEEE Int. Solid-State Circuits Conf. (ISSCC) Dig. Tech. Papers, San Francisco, CA, USA, Feb. 2015, pp. 1 - 3
- [5] W. Jung, S. Oh, S. Bang, Y. Lee, D. Sylvester, and D. Blaauw, "A 3nw Fully Integrated Energy Harvester Based on Self-Oscillating Switched-Capacitor DC-DC Converter" in IEEE Int. Solid-State Circuits Conf. (ISSCC) Dig. Tech. Papers, San Francisco, CA, USA, Feb. 2014, pp. 398 - 399.
- [6] S. Bandyopadhyay and A. P. Chandrakasan, "Platform Architecture for Solar, Thermal, And Vibration Energy Combining with MPPT and Single Inductor" IEEE J. Solid-State Circuits, vol. 47, no. 9, pp. 2199 - 2215, Sep. 2012.
- [7] D. Bol, E. H. Boufouss, D. Flandre, and J. D. Vos, "A 0.48 mm^2 5 μW -10mw Indoor/Outdoor PV Energy-Harvesting Management Unit in a 65nm SoC Based on a Single Bidirectional Multi-Gain/Multi-Mode Switched- Cap Converter with Supercap Storage" in Proc. 41st Eur. Solid- State Circuits Conf. ESSCIRC (ESSCIRC), Graz, Austria, Sep. 2015, pp. 241 - 244.
- [8] Savanth, A. S. Weddell, J. Myers, D. Flynn and B. M. Al-Hashimi, "Integrated Reciprocal Conversion With Selective Direct Operation for Energy Harvesting Systems" in IEEE Transactions on Circuits and Systems I: Regular Papers, vol. 64, no. 9, pp. 2370-2379, Sept. 2017.